PROCEEDINGS, 41st Workshop on Geothermal Reservoir Engineering
Stanford University, Stanford, California, February 22-24, 2016
SGP-TR-209

Introducing a Short-Term Holistic Approach for More Efficient Heat Pump Systems

Christopher Steins, Michael Heger, Reinhold Kneer

steins@wsa.rwth-aachen.de, michael.heger@rwth-aachen.de, kneer@wsa.rwth-aachen.de

Keywords: borehole heat exchanger, coaxial borehole heat exchanger, short-term model, heat transfer, cylinder source theory, heat pump, large volume borehole heat exchanger

ABSTRACT

Ground-coupled heat pump systems (GHPS) become increasingly popular for providing buildings with heating and cooling, replacing existing boilers fired by fossil fuels. Focusing on the heating purpose, a heat pump uses a small amount of electrical energy to upgrade low temperature heat from the ground within a thermodynamic cycle to the target temperature of the heating network. With respect to the thermodynamic concept, the optimizing goal of such processes is a high and quasi-constant inlet temperature into the heat pump, reducing the amount of electrical energy to deliver the same amount of heat to the network. In this paper, a short-term model of a borehole heat exchanger (BHE) is presented, introducing a holistic approach to optimize the GHPS. The model is based on a large volume coaxial BHE, which, in addition, offers a favorable larger volume compared to standard (double-) U-pipes. A hybrid approach using a combined finite-volume and an analytical scheme thereby enables the continuous simulation of temperature fields within the pipe and the surrounded volume with respect to the operation of the heat pump and the characteristic parameters of the system. Thus, it becomes possible to develop a deep understanding of the impact of heat pump operation on the ground's and working fluid's temperature and vice versa as well as the efficiency dependencies of the overall system, which will lead to a more efficient use of GHPS.

1. INTRODUCTION

The demand of space heating and warm water is significant and accounts for more than a half of the energy consumption of typical U.S. homes and other buildings (EIA, 2009). Primary, natural gas is burned to provide the necessary heat, which contributes to a negative environmental impact, due to its emissions. In contrast, borehole heat exchangers (BHE) in combination with a heat pump provide sustainable heat for buildings and are less costly on their life-cycle than other systems, but the investment costs, especially for the wellbore and the BHE, still prevent these systems to reach major market shares. Although heat pumps benefit from the temperature stability of the ground (Javed and Claesson, 2011; Maestre et al., 2015), this advantage of ground-coupled heat pump systems has rarely been used, so far, because present systems still fluctuate strongly in temperature or can often not meet the economic targets. To overcome the drawback of drilling costs and thus, allowing more clients to afford these systems, future systems must follow a holistic approach to exploit all technical and economic opportunities. Not only the single parts must be developed, the optimization strategy has to be based on the interrelationship of all related parts, including ground system, heat pump, residential heating network, and power supply.

A crucial aspect in this context is the detailed understanding of the part load behavior (short-term behavior) of the BHE to forecast the inlet temperature into the heat pump under certain operation schemes and to optimize the control strategy of the overall system. Therefore, this paper includes two major objects of this overall task: first, a new type of BHE is considered: a large volume borehole heat exchanger (LVBHE) shows favorable results with regard to short-term behavior (Hamann et al. 2013; Kuebert, 2011)). Second, an adopted short-term model is presented, which enables the analysis of the temperature field and heat flows within and around the LVBHE for times of up to 100 hours using step widths of minutes.

2. LARGE VOLUME BOREHOLE HEAT EXCHANGER

Typical BHE are single- and double-U-pipes with inner diameters between 25mm and 32mm or coaxial pipes with an inner diameter of 56mm, which are inserted into a borehole with a total depth of 50-150m and which are thermally connected to the borehole wall with cement-like grouting material (GM) (Florides and Kalogirou, 2007). These types reach depths, where the temperature of the ground is only affected by the surface conditions in timescales of years and thus, separates it from other ground-coupled systems, e.g. surface collectors, heat baskets or heat piles (De Carli et al., 2010). All systems use a liquid heat carrier medium (fluid) flowing through the pipes to absorb the heat from the ground and to transfer it to the heat pump, where the heat of the ground is shifted onto a usable temperature level for the heating network.

LVBHE differ from typical BHE by the amount of fluid per unit length inside the BHE, which is considerably larger. A larger total volume acts as a heat storage, which can be activated without delay, in contrast to the heat in the ground and thus, can provide peak demands, for example. Furthermore, LVBHE can be loaded while the system is in standstill over a longer time-span in contrast to BHE with smaller volume and therefore, do not need to extract the heat from the ground, immediately. Moreover, the cycle-time of the heat carrier fluid is increased, giving the heat pump longer access to the stored heat.

In order to maximize the inner volume of a BHE within a given borehole, an axially symmetric coaxial type is most appropriate, because it offers the largest length related volume and it is simple. A coaxial BHE is made from an outer pipe and a concentrically mounted inner pipe (Fig. 1). In operating mode the fluid flows down the annulus, absorbs the heat from the surrounding ground ($\dot{q}'_{GM\rightarrow AN}$) through the outer pipe's wall and returns through the inner pipe to the heat pump on the surface. For this study, the reference size is based on an existing model (Steins and Kneer, 2013). The outer pipe diameter is 140mm with a wall thickness of 5.4mm, while the inner pipe diameter is 40mm with a wall thickness of 3.5mm. Both pipes are made from Polyethylene (PE-HD) with a thermal conductivity of k_P=*0.42 W/mK*. Comparing the resulting inner volume with other typical BHE, the reference LVBHE is at least four times larger in inner volume and thus, is able to store four times more heat for the same temperature difference (Fig. 2).

However, larger inner volumes lead to lower flow velocities and hence, to a reduced heat transfer rate. This limitation must be considered, when using LVBHE.

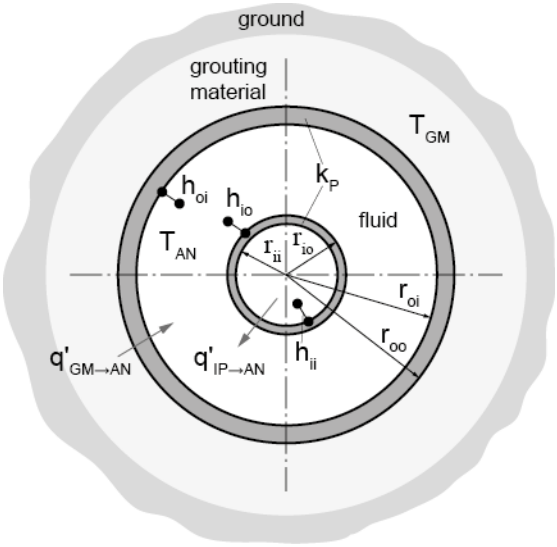

Fig. 1: Cross-section of coaxial BHE with characteristic parameters

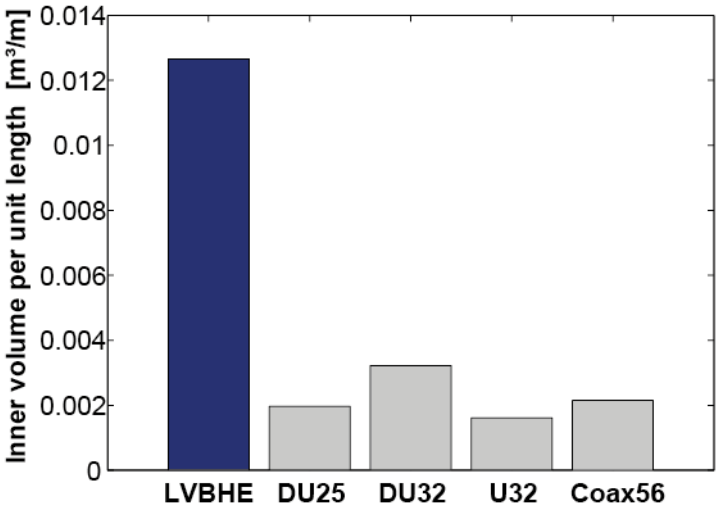

Fig. 2: Comparison of inner volume of different BHE with LVBHE. (Numbers indicate the inner diameter of the largest pipe. 'DU' means Double-U-Pipe, 'U' means U-Pipe and 'Coax' means regular coaxial BHE.)

2.1 Heat transfer in coaxial LVBHE

The effectiveness and performance of a BHE depends on the ability to absorb heat and to deliver it to the heat pump. The ground around a BHE is a large natural heat storage with a specific volume related heat capacity and a BHE is the necessary device to extract this heat for further usage. Thereby, the main heat transfer takes place from the solid body (grouting material and ground) to a flowing fluid within an enclosed circular volume. The underlying processes depend on time and location as well as on thermal and operating properties (Fig. 1). The GM fixes the BHE within the borehole, connects it thermally to the ground, and acts as a sealing for ground water levels. Different GMs are available, whereas the most expensive ones are optimized in terms of its heat conductivity. Besides the heat transfer between the fluid in the annulus and the ground, heat transfer takes also place between the inner pipe and the annulus, keeping a portion of the extracted heat circulating within the BHE ($\dot{q}'_{IP\rightarrow AN}$). In general, heat transfer from the ground into the annulus shall be high, while the internal heat transfer should be small.

In a BHE setup, the heat transfer rate $\dot{q}'$ from the solid ground must overcome the thermal resistances of the outer pipe and the convective heat transfer coefficient *h* (HTC). The transient behavior of the pipe's material is neglected, due to its small wall thickness:

$$q'_{GM\rightarrow AN} = \frac{2\pi}{\frac{1}{h_{oi}\cdot r_{oi}}+\frac{1}{k_P}\cdot\ln\left(\frac{r_{io}}{r_{oi}}\right)}\cdot\left(T_{GM}\,(z,t)-T_{AN}(z,t)\right) \quad (1)$$

Although the pipe's material may also be varied in terms of heat conductivity and thickness, the HTC at the outer wall (*oi*) is a key factor for LVBHE as it depends on the actual cross-sectional area of the annulus and the operating conditions (volume flow rate). In a dimensionless form, the HTC is represented by Nusselt-correlations (Nu), which are available for different conditions and which basically depend on Reynolds-number (Re), hydraulic diameter ($d_h = 2(r_{oi}-r_{io})$) of the annulus and Prandtl-number (Pr):

$$Nu = \frac{h\cdot d_h}{k_{fluid}} = f(Re,\mathrm{Pr}) \quad (2)$$

Nusselt-correlations for annuli and pipes were taken from the open literature, e.g. VDI Waermeatlas (2013).

Especially, the flow conditions – laminar or turbulent – significantly affect Nusselt-number and thus, the HTC. A Reynolds-number of 2300 is seen as a critical value for the onset of turbulent flow (VDI Waermeatlas, 2013). The Reynolds-number of the annulus is expressed as a function of the volume flow rate, the fluid's viscosity and the limiting radii:

$$Re_{AN} = \frac{2 \cdot \dot{V}}{\pi \cdot (r_{oi} + r_{io}) \cdot \upsilon(T)} \tag{3}$$

Because of the larger dimensions, the flow within the annulus section of LVBHE is primary laminar, or at least with minor flow fluctuations at larger volume flow rates (Fig. 3), while the flow within the inner pipe can be seen turbulent.

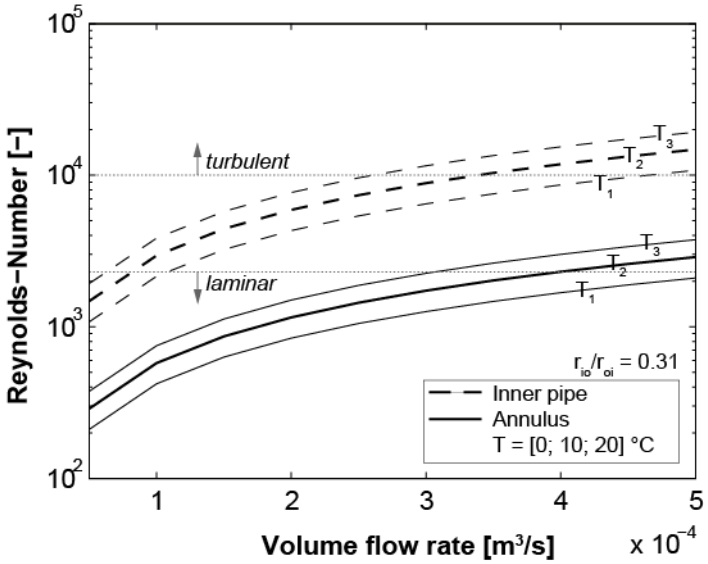

Fig. 3: Reynolds-numbers in reference LVBHE as function of volume flow rate and fluid temperature.

When the fluid enters the annulus at the inlet, a boundary layer develops, which acts as increasing thermal resistance. Depending on the actual setup and operating conditions, the HTC may drop by approximately 50% within the first twenty meters of the pipe length. Additionally, the HTC in laminar flows is generally lower than in turbulent flows, due to the significantly lower radial fluid exchange and heat transfer fraction by mass transport. Nevertheless, the thermal resistance of the HTC must be set into relation to the thermal resistance of the GM and the ground. The characteristic number to describe this relation is the Biot-number (Bi) (compare Fig. 7 and Eq. (19)-(21)):

$$Bi = \frac{h_{oi} \cdot r_{oi}}{k_{GM}} \tag{4}$$

Thereby, the thermal resistance caused by the HTC becomes only relevant, if the Biot-number is much smaller than one, and is less relevant, if the Biot-number is much greater than one, respectively. Hence, the heat transfer within LVBHE should be examined in detail to avoid an additional thermal resistance. An option might be fittings, mounted within the annulus, to enforce frequent break-ups of the laminar boundary layers and additional turbulences (Steins and Kneer, 2013).

3. MODELING

The operation of a GHPS is highly dynamic in terms of the thermal behavior of the ground and the BHE. For a proper understanding of the dependencies and an efficient design, accurate modeling of the BHE is crucial. When it comes to a more detailed view on the modeling of GHPS, two directions must be distinguished: long-term and short-term modeling. Until the end of the last century, research has been focused on long-term simulations, which estimate the thermal response of the ground and BHE over a time-span of years. Long-term simulations aim at the sustainable operation of systems over their lifetime and a quick design, but are limited in forecasting the immediate response of the BHE (Javed et al., 2009). Modelling fundamentals have been introduced by Ingersoll et al. (1954) and analytical as well as numerical solutions have been developed by several researches over the following decades (e.g. Hellstroem, 1991). These models usually are based on the line source theory, which covers the interior of the borehole (BHE, heat carrier fluid, grouting material) as a one-dimensional line with a constant, length related heat flux. By introducing the cylinder source theory, the issue of constant heat flux could be handled. Nevertheless, both approaches neglect the interior of the wellbore and especially the heat capacity of the fluid within the BHE (Javed et al., 2009).

In 1999, Yavuzturk introduced the first short-term model to overcome the limitations of long-time models. As Hellstroem did for the long-term models 10 years before, Yavuzturk developed numerically-generated g-functions for the interior part of the wellbore (Yavuzturk and Spitler, 1999). However, these functions also have to be calculated beforehand and thus, lack in flexibility. Many researches adopted the importance of short-term models and developed different numerical and analytical solutions or extensions of existing models (Young, 2001; Lamarche and Beauchamp, 2007; Lamarche, 2013; Javed and Claesson, 2011).

Capacity resistance models have been developed to include fluid heat capacity and fluid flow pattern (De Carli et al., 2010; Zarrella et al., 2011; Maestre et al., 2015), while three-dimensional modeling enables detailed analysis of small areas of points of interest under the drawback of large computational times (compare Paerisch et al., 2015).

All these models have their specific advantages and usually represent reference cases well. By introducing LVBHE, the fluid's heat capacity becomes even more relevant and according to Javed et al. (2009), the analysis of short-term effects is crucial for further optimizations. For this reason, a hybrid model has been developed that takes all effects influencing the performance of LVBHE into account.

3.1 The hybrid model approach

The aim of the presented model is the transient simulation of the short-term temperature field specifically within coaxial LVBHE to enable the analysis of the heat balance over the length of the BHE and the prospection of the outlet temperature over time. The model is coded in Matlab© and allows the calculation of about 100 hours of continuous operation of a BHE with computational times of minutes on a standard PC. The main characteristics are the handling of variable material properties and operating conditions, the consideration of the inner heat exchange between the two flow sections and the simulation of cyclic operation. Moreover, the simulation tool is easily extendable to attach a detailed heat pump simulation, for example, continuing the holistic approach.

The final results are time and location dependent temperatures which help to understand the influence of system parameters in order to achieve a higher effectiveness of BHE and heat pump. Therefore, the model is based on heat balances, only, and does not simulate the flow field. Empirical correlations, like the Nusselt-correlations (see 2.1), fulfill the requirements for convective heat transfer. Additionally, the axial symmetry of the coaxial pipe simplifies the model structure, such that a one-dimensional structure for the interior and a two-dimensional structure for the exterior is sufficient. Three-dimensional ground characteristics are neglected, here.

Overall, the model is subdivided into three separated spaces, the BHE, the grouting material and the ground (Fig. 4). The first two parts are simply discretized and allow the use of the finite-difference method, while the last part is based on the cylinder source theory.

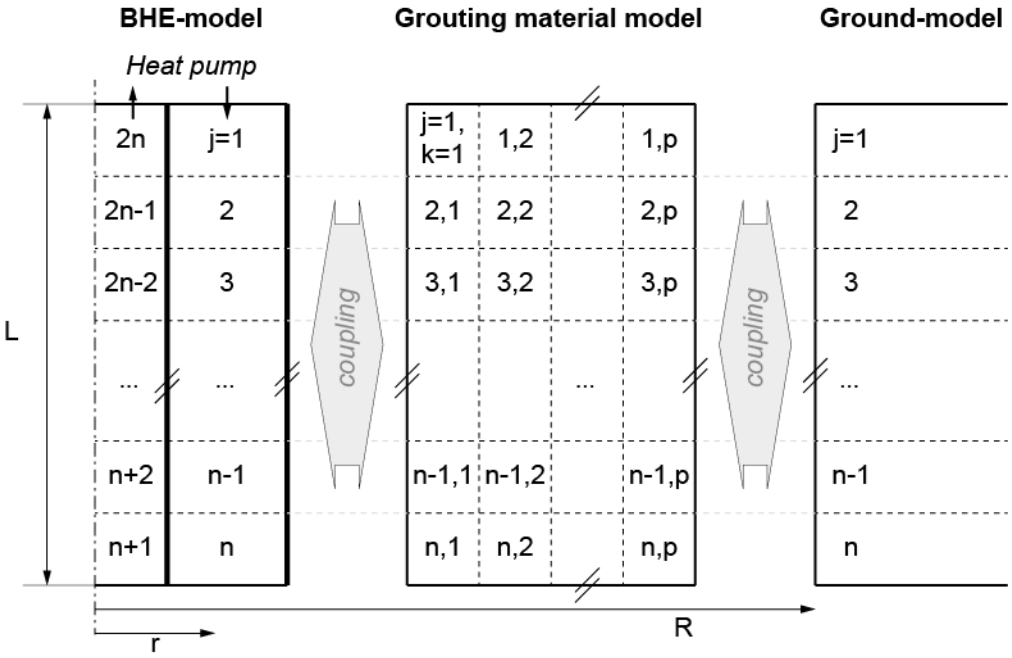

Fig. 4: Overview about the hybrid model with its separate parts: BHE-model, grouting material model and ground-model.

3.1.1 The BHE-model

Due to the symmetric structure of the coaxial pipe, the inner volume of the BHE is modeled in a 1D-structure and discretized lengthwise starting at the inlet of the annulus and ending at the outlet of the inner pipe (Fig. 6).

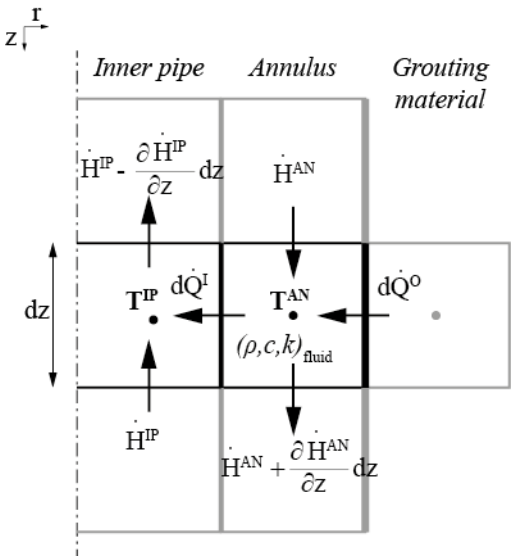

Fig. 5: Energy balance of BHE-model.

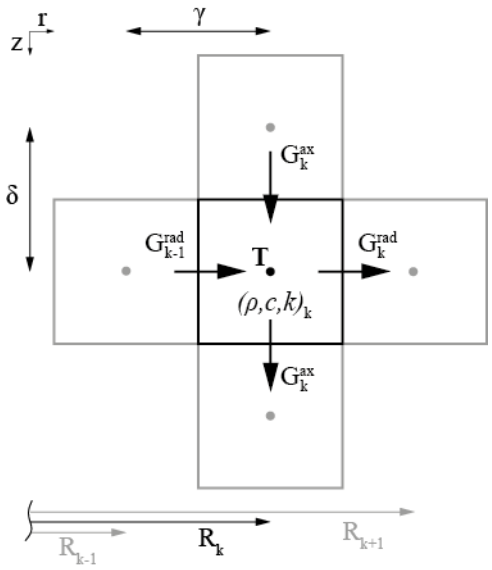

Fig. 6: Energy balance of grouting material model.

Each step represents a control volume with its individual energy balance (Fig. 5). In summary, the differential equations for both parts are:

$$0 = C^{AN}\frac{\partial T^{AN}}{\partial t} + \dot{C}\frac{\partial T^{AN}}{\partial z} + G^{O}(T^{AN} - T^{O}) + G^{I}(T^{AN} - T^{IP}) \quad \text{(Annulus)} \tag{5}$$

$$0 = C^{IP}\frac{\partial T^{IP}}{\partial t} - \dot{C}\frac{\partial T^{IP}}{\partial z} + G^{I}(T^{IP} - T^{AN}) \quad \text{(Inner Pipe)} \tag{6}$$

with

$$C^{AN} = \rho_{fluid} \cdot c_{fluid} \cdot \pi \cdot (r_{oi}^2 - r_{io}^2) \tag{7}$$

$$C^{IP} = \rho_{fluid} \cdot c_{fluid} \cdot \pi \cdot r_{ii}^2 \tag{8}$$

$$\dot{C} = \rho_{fluid} \cdot c_{fluid} \cdot \dot{V} \tag{9}$$

$$G^{O} = 2\pi \cdot \left[\frac{1}{r_{oi} \cdot h_{oi}} + \frac{1}{k_P} \cdot ln\left(\frac{r_{oi}}{r_{io}}\right)\right]^{-1} \tag{10}$$

and

$$G^{I} = 2\pi \cdot \left[\frac{1}{r_{ii} \cdot h_{ii}} + \frac{1}{k_P} \cdot ln\left(\frac{r_{io}}{r_{ii}}\right) + \frac{1}{r_{io} \cdot h_{io}}\right]^{-1} \tag{11}$$

The HTC on both walls of the annulus is assumed to be equal, which is based on the simplification of equal heat flux on both sides of the inner wall: $h_{oi} = h_{io}$. More details about the numerical approach can be found in the appendix.

3.1.2 The grouting material model

The volume around the BHE is discretized in two dimensions, whereat each cell represents the thermal capacity of a ring volume (Fig. 6). Thereby, the spacing of the grid is constant in either axial or radial direction. In axial direction the spacing equals the spacing of the annulus (δ), which in total gives n layers. In radial direction the number of layers p may be chosen as well as its width γ, but shall be limited to an individual extend by the user.

Each cell contains the temperature information of a point in time and is influenced by the radial and axial heat flow to and from the four neighboring cells as well its own internal energy U:

$$\frac{\partial(dU)}{\partial t} = \sum d\dot{Q}^{rad} + \sum d\dot{Q}^{ax} \tag{12}$$

Thereby, the temperature of each cell and each point in time depends on the temperature of is neighboring cells. However, the numerical effort is high due to $n \cdot p$ coupled equations. Therefore, an implicit discretization of the axial heat flow is neglected, because the magnitude may be assumed to be lower than in radial direction (Heger, 2014). More details about the numerical approach can be found in the appendix.

3.1.3 The ground model

By extracting heat from the ground via BHE, the temperature drops deeper in the near field of the BHE than in the far field, due to the larger specific volumetric heat capacity of a ring with discrete radial extent. However, the heat recharge of the near field is provided by the far field and thus, this needs to be modeled according to the temperature change of the near field. While a discretization method leads to a higher consumption of computational time and storage, the ground model in this approach follows the idea of Huber and Schuler (1997), who approximated the outer boundary conditions by analytical functions (Heger, 2014). Thereby, the temperatures at the outer boundary of the grouting material model are calculated from the superposition of the ground's step response functions by discrete heat flow steps.

Mathematically, the response function $y(t)$ is determined by the convolution of an impulse response $g(t)$ with an arbitrary input signal $u(t)$:

$$y(t) = \int_0^t u(x) \cdot g(t-x)dx \tag{13}$$

Here, the input signal is a heat flux $\dot{q}'$ through a cylindrical wall (outer boundary of the grouting material model) resulting from an infinite homogenous medium (ground) with an initial temperature T_0 and the response function is the time and location dependend temperature on the wall rim. The response function in Eq. 21 can be approximated by replacing the integral with a discrete sum of input pulses. If the differences between sequent pulses are used as input signal instead of the pulses themselves, the impulse response *g(t)* can be replaced with the step response *h(t)* (Heger, 2014):

$$\hat{y}(t) = \sum_{i=1}^{m}[(u_i - u_{i-1}) \cdot h(t-t_i)] \tag{14}$$

In this model, the step response function of the temperature is taken from Carslaw and Jaeger (1959), who developed a solution for transient heat conduction into a radial infinite space via Laplace transformation:

$$H(Fo,\mathcal{X}) = (T-T_0)\cdot\frac{k_G}{\dot{q}'} = \frac{1}{\pi^2}\underbrace{\int_0^\infty \left(e^{-Fo\cdot\omega^2}-1\right)\cdot\frac{1}{\omega^2}\cdot\overbrace{\frac{J_0(\mathcal{X}\omega)Y_1(\omega)-Y_0(\mathcal{X}\omega)J_1(\omega)}{J_1^2(\omega)+Y_1^2(\omega)}}^{B(\omega,\mathcal{X})}\cdot d\omega}_{I(\omega,\mathcal{X},\mathrm{Fo})} \tag{15}$$

whereby, $\omega := u \cdot R$, the Fourier number $Fo = (k_G/\rho_G \cdot c_G)\cdot t/R^2$, the dimensionless radius $\mathcal{X} = r/R$ and the dimensionless step response function is H. J_ν and Y_ν are Bessel- and Neumann functions of the order ν. This approach is able to give solutions for high-resolutions in time, which is favored in this short-term model (Heger, 2014). More details about the numerical approach can be found in the appendix.

3.1.4 Coupling of the model parts

The three model parts are calculated separately to reduce the numerical effort and must be coupled to work together. Because the temperature of the first cell of the grouting model is not available at a present time step, it must be estimated to close the energy balance around the annulus cell of the BHE-model (Heger, 2014). Therefore, the energy balance around the first grouting cell is simplified by neglecting the axial heat flux. Furthermore, the temperature of the annulus cell at first is forecasted implicitly by the stored temperature information of the previous time step:

$$\tilde{T}_{ij}^{AN} = T_{i-1j}^{AN} + \frac{\tau\dot{C}}{C_{AN}}\cdot\left(T_{i-1j-1}^{AN} - T_{i-1j}^{AN}\right) \tag{16}$$

Combining this information the estimated temperature of the first cell in the grouting model becomes

$$\tilde{T}_{ij}^{GM} = \frac{\frac{C_1}{\tau}T_{i-1j1}^{GM} + G_j^O\tilde{T}_{ij}^{AN} + G_1^{rad}T_{i-1j2}^{GM}}{\frac{C_1}{\tau} + G_j^O + G_j^{rad}} \tag{17}$$

Now, the calculation of the BHE-model can be finished for this time step.

The grouting model, being calculated after the BHE model, now can access the temperature information of the annulus in the present time step. The final calculation of the first cell in the grouting model also is simplified regarding the axial heat flux and is calculated according to Eq. 33 with an averaged annulus temperature value, using the present and the previous time step.

The third part model (ground model) needs a length related heat flux as initial input parameter. This is calculated from the last two cells of the grouting model in the present time step, whereat the temperature of the last cell is defined as the present ground temperature $T_{ijp}^{GM} \coloneqq T_{i-1j}^{G}$:

$$\dot{q}_j'(t) = \frac{G_{p-1}^{rad}}{\delta} \cdot \left(T_{ijp}^{GM} - T_{ijp-1}^{GM}\right) \tag{18}$$

Last, the boundary condition of the inlet into the BHE is mandatory. In the model presented the heat pump is not modeled, but acts in reducing the temperature of the BHE outlet by a user defined value ΔT (comparable to a thermal response test). Thus, the inlet temperature into the BHE in the present time step is calculated via $T_{i1} = T_{i-12n} - \Delta T$.

3.2 Validation of the model

Validation of the model has not been conducted with a specifically designed in-situ reference case, but analytical expressions are available to validate the convolution model of the ground. Mundry (1966) provides analytical expressions for this case:

If Fourier numbers are small ($\sqrt{Fo}/\mathcal{X} < 0.5$), the approximation is

$$\frac{T-T_0}{T_{fluid}-T_0} \approx \frac{1}{\sqrt{\mathcal{X}}} \cdot \left[1 - erf\,\frac{\mathcal{X}-1}{2\sqrt{Fo}}\right] - \frac{1}{\sqrt{\mathcal{X}}} e^{\left(Bi(\mathcal{X}-1)+Bi^2 Fo\right)} \cdot \left[1 - erf\left(\frac{\mathcal{X}-1}{2\sqrt{Fo}} + Bi\sqrt{Fo}\right)\right] \tag{19}$$

with $10 \leq Fo \leq 1000$ and $Bi \geq 1$ it becomes

$$\frac{T-T_0}{T_{fluid}-T_0} \approx \frac{Bi(f-\ln(\mathcal{X}))}{1+Bi \cdot f} \tag{20}$$

with

$$f = 0.83 - \frac{0.092}{\sqrt[3]{Bi}} + 0.465 \cdot \ln(Fo) \tag{21}$$

For $\mathcal{X} = 1$ the simulation results can be confronted with the analytical approximation, which show a well representation, in Fig. 7:

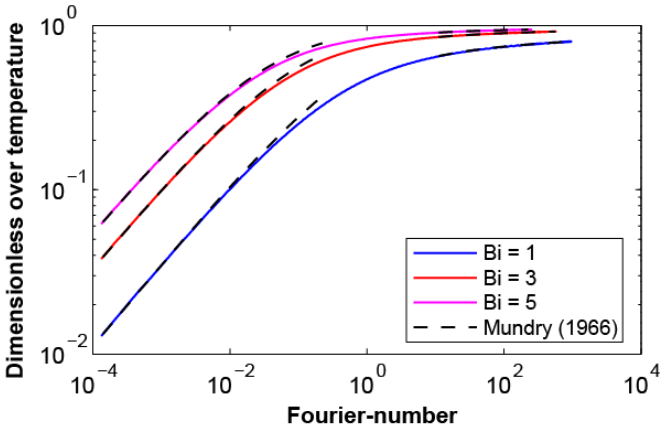

Fig. 7: Validation of the ground model based on the analytical approximation by Mundry (1966) (Heger, 2014).

Validation of the short-term behavior will be conducted within future work by analyzing the temperature field in high-resolution under laboratory conditions.

4. RESULTS

As described in the introduction, the model presented is not yet able to simulate a complete GHPS, but enables the analysis of BHE behavior. Therefore, the following results (Fig. 8+9) shall give a first impression of what the model aims for and is able to provide. A final analysis of a specific case shall not be given, here. The focus of the model are time and location resolved information about the temperature distribution within the BHE and the heat flux between the first layer of the grouting material and the BHE as well as the heat flux between annulus and inner pipe.

In the example scenario, the dimensions of the BHE are set as described in 2, the initial temperature is 10°C, the volume flow rate 0.5 l/s and the temperature drop of the heat pump shall be fixed to 3K. In Fig. 8, a 100m long pipe is simulated over time and the figure shows the temperature profile at specific times within the annulus, as well as the temperature difference to the first layer of the grouting material, which is nearly proportional to the heat flux. Especially, the non-equal heat transfer over the pips's length can be analyzed, here. Fig. 9 compares the temperature distribution at 5m depth for different length of the LVBHE over a time-span of one hour. It primary shows the temperature drop from the heat pump after a single cycle, which is – of course – shorter at a shorter length.

As soon the model is validated also for the standstill behavior, the data may help to identify the best length and flow conditions within the pipe by a parameter study and will increase the understanding of LVBHE.

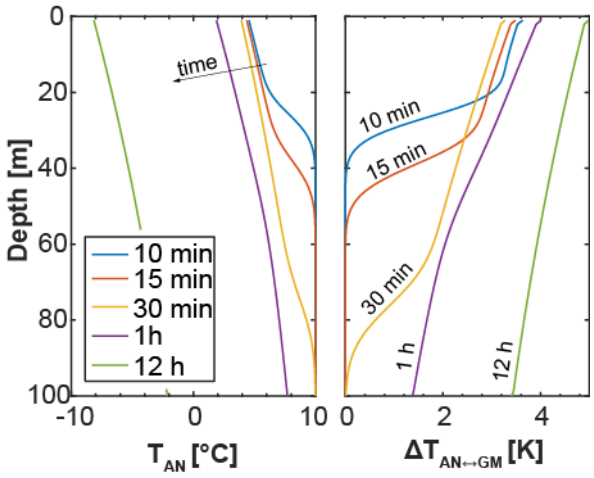

Fig. 8: Temperature distribution within the annulus of a 100m long LVBHE at different time steps (left); coincident temperature difference between annulus and first grouting material layer (right).

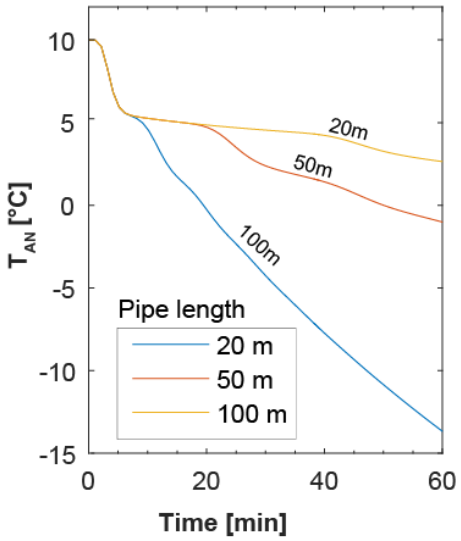

Fig. 9: Temperature distribution within the annulus over time for different length of a LVBHE at 5m depth.

5. CONCLUSION AND OUTLOOK

In this paper, a hybrid model approach is presented to simulate the short-term behavior of coaxial LVBHE. Moreover, LVBHE have been introduced as a specialized form of BHE, offering a larger inner volume per unit length and so, the ability to store more heat within the BHE. Thereby, the heat stored within the fluid is quicker accessible and may reduce large fluctuations at the outlet of the LVBHE (inlet of the heat pump), while lower flow velocities may reduce the heat transfer. This trade-off can be solved by the adaption of the design and the operation of BHE and will require more research to extract the most suitable setup.

The hybrid model has been developed to analyze the impact of the system's design parameters in detail. The model is built modular for further extension and detailed settings, enables quick simulations (under one hour) of a time interval up to 100 hours and outputs temperature information of minutes in every single location within or outside the LVBHE. Although the validation has not been finished, yet, and the detailed heat pump model is still missing, the model may already be used to identify positive and negative characteristics of coaxial LVBHE.

The next steps will concentrate on the experimental validation of the short-term behavior and the integration of a realistic heat pump model to evaluate the interdependencies between LVBHE and heat pump with regard to the overall system performance. Moreover, an exergy analysis has already been adapted to the model, which results are evaluated at the time of writing.

APPENDIX

To 3.1.1

The differential quotients are approximated numerically using a time step τ and a length step δ. Thereby, the time dependent deviatives are transformed into:

$$\frac{\partial T}{\partial t} = \frac{1}{\tau}(T_i - T_{i-1}) \tag{A1}$$

while the time dependent temperatures are further averaged by the Trapezoidal rule:

$$T(t) \approx \frac{1}{2}(T_i + T_{i-1}) \tag{A2}$$

The volume flow rate is constant per time step and so, it is independent from the approximation.

The length related differential quotient is approximated by an upwind-differential scheme for stability reasons (Heger, 2014). Due to the 1D-structure, the length index is defined in its section (inner pipe or annulus, Fig. 4):

$$T_{ij} \coloneqq \begin{cases} T^{AN}(z = \delta \cdot (j-1) & \text{with } j = 1, \dots, n \\ T^{IP}(z = \delta \cdot (2n-j) & \text{with } j = n+1, \dots, 2n \end{cases}$$

Finally, the differential quotients are transformed into:

$$\left.\frac{\partial T^{AN}}{\partial z}\right|_i \approx \frac{1}{\delta}\left(T_{ij} - T_{ij-1}\right) \quad \text{with } j = 1, \dots, n \tag{A3}$$

$$\left.\frac{\partial T^{IP}}{\partial z}\right|_i \approx \frac{1}{\delta}\left(T_{ij-1} - T_{ij}\right) \quad \text{with } j = n+1, \dots, 2n \tag{A4}$$

By replacing the differential quotients within Eqs. 5 and 6 with the numerical approximations, a set of linear equations can be formed, which result is a vector of length *2n* for the discrete temperatures within the BHE. The inversion of the component matrix is then calculated for every time step.

To 3.1.2

By using the Trapezoidal rule for the differential quotient of time, the numerically approximated heat balance for each cell becomes:

$$\frac{C_k}{\tau}\left(T_{ijk} - T_{i-1jk}\right) = \frac{G_{k-1}^{rad}}{2}\left(T_{ijk-1} + T_{i-1jk-1} - T_{ijk} - T_{i-1jk}\right) - \frac{G_k^{rad}}{2}\left(T_{ijk+1} + T_{i-1jk+1} - T_{ijk} - T_{i-1jk}\right) + G_k^{ax}\left(T_{i-1j-1k} - 2T_{i-1jk} + T_{i-1j+1k}\right) \tag{A5}$$

with the parameters G^x containing the values of the heat conduction:

$$G_k^{rad} \approx \frac{2\pi r_k k_{GM} \delta}{\gamma} \tag{A6}$$

$$G_k^{rad} \approx \frac{2\pi r_k k_{GM} \gamma}{\delta} \tag{A7}$$

and the parameter *C* as the value of the heat capacity of the cell:

$$C_k = \rho_{GM} \cdot c_{GM} \cdot 2\pi r_k \gamma \delta \tag{A8}$$

As within the BHE-model a set of linear equations can be formed, which result is a matrix of size *np* for the discrete temperatures within the grouting material. The inversion of the component matrix is also calculated for every time step.

To 3.1.3

An analytical expression for the integral *I* is not available. In order to solve it numerically, it is split into three parts: $\omega \in [0, \omega_1]$, $\omega \in [\omega_1, \omega_2]$ and $\omega \in [\omega_2, \infty]$.

For small values of ω, the exponential function evaluates close to one. Numerical errors resulting from the subtraction of nearly equal numbers can be avoided by approximating the exponential function with a Taylor approach of order two around zero (Heger, 2014). This leads to

$$\left(e^{-Fo\cdot\tilde{\omega}^2}-1\right)\cdot\frac{1}{\tilde{\omega}^2}\approx -Fo \tag{A9}$$

while ω_1 can be set to $\omega_1 \leq \sqrt{0.01/Fo}$, evaluted by an error analysis of the Taylor approximation.

For large arguments, the Bessel- and Neumann functions can be approximated by (Burg at al. (2013)):

$$J_\nu(x)\approx\sqrt{\frac{2}{\pi x}}\cos\left(x-\nu\frac{\pi}{2}-\frac{\pi}{4}\right) \tag{A10}$$

$$Y_\nu(x)\approx\sqrt{\frac{2}{\pi x}}\sin\left(x-\nu\frac{\pi}{2}-\frac{\pi}{4}\right) \tag{A11}$$

Further simplifications by the use of trigonometry theorems finally lead to the expression

$$B\approx-\cos\big((\mathcal{X}-1)\omega\big) \tag{A12}$$

and by focusing on the relevant location on the boundary ($\mathcal{X}=1$) it becomes (Heger, 2014)

$$B\approx-\cos(0)=-1 \tag{A13}$$

For high values of ω, the exponential expression disappears and the solution of the integral becomes

$$\int_{\omega_2}^{\infty}\frac{1}{\tilde{\omega}^2}d\tilde{\omega}=\frac{1}{\omega_2} \tag{A14}$$

In summary, the step response function H on the boundary ($\mathcal{X}=1$) is

$$H(Fo,\mathcal{X}=1)\approx\int_0^{\omega_1}Fo\cdot d\tilde{\omega}-\int_{\omega_1}^{\omega_2}\left(e^{-Fo\cdot\tilde{\omega}^2}-1\right)\cdot\frac{1}{\tilde{\omega}^2}\cdot d\tilde{\omega}+\frac{1}{\omega_2} \tag{A15}$$

and the convolution sum finally becomes

$$T_{ij}=T_0-\frac{1}{k_G}\sum_{i^*=1}^{i-1}\left[\left(\dot{q}'_{i^*j}-\dot{q}'_{i^*-1j}\right)\cdot H(Fo_i-Fo_{i^*},\mathcal{X}=1)\right] \tag{A16}$$

NOMENCLATURE

Variables		**Subscripts**		**Greek symbols**	
c	Spec. heat capacity (kJ/kgK)	AN	Annulus	γ	Radial cell width (m)
d_h	Hydr. Diameter (m)	ax	Axial	δ	Axial cell length (m)
h	Heat transfer coefficient (W/m²K)	G	Ground	ρ	Density (kg/m³)
J	Bessel function	GM	Grouting material	ν	Kin. Viscosity (m²/s)
k	Heat conductivity (W/mK)	i	Index of time	τ	Time step (sec)
$\dot{q}'$	Heat flux (W/m)	ii	Wall on inner pipe		
$\dot{Q}$	Heat flow (W)	io	Wall on inner pipe in annulus		
r	Radius (m)	IP	Inner pipe		
R	Reference radius (m)	j	Index of axial length		
t	Time (sec)	k	Index of radial length		
T	Temperature (°C)	n	Maximum axial index		
T_0	Initial temperature (°C)	O	Outside (here: grouting material)		
ΔT	Temperature drop in heat pump (°C)	oi	Inner wall on outer pipe		
$\dot{V}$	Volume flow rate (m³/s)	p	Maximum radial index		
Y	Neumann function	P	Pipe		
z	Variable of depth	rad	Radial		
		sim	Simulation		
		TRT	Thermal response test		

REFERENCES

Burg, K., Haf, H., Wille, F., and Meister, A.: Funktionentheorie, *2nd Issue*, Springer Fachmedien Wiesbaden, (2013).

Carslaw, H.S., and Jaeger, J.C.: Conduction of Heat in Solids, *2nd Issue*, Oxford University Press, (1959).

De Carli, M., Tonon, M., Zarrella, A., and Zecchin, R.: A computational Capacity Resistance Model (CaRM) for Vertical Ground-coupled Heat exchangers, *Renewable Energy*, **35**, (2010), 1537-1550.

Eskilson, P.: Thermal analysis of heat extraction boreholes, *Doctoral thesis*, Lund University, Sweden, (1987).

Florides, G., and Kalogirou, S.: Ground Heat Exchangers: a Review of systems, models and applications, *Renewable Energy*, **32**, (2007), 2461-2478.

Hamann, J., Noering, W., Walker-Hertkorn, S., and Wagner, S.: Praktische Ergebnisse des Einsatzes von Koaxialsonden großen Volumens (german), *brr Leitungsbau, Brunnenbau, Geothermie (Sonderheft Geothermie)*, (2013), 40-43.

Heger, M.: Numerische Berechnung des instationären Temperaturfeldes einer großvolumigen koaxialen Erdwärmesonde, *Diploma thesis*, RWTH Aachen University, (2014).

Hellstroem, G.: Ground Heat Storage. Thermal Analysis of Duct Storage Systems: Theorie, *Doctoral thesis*, University of Lund, Sweden, (1991).

Huber, A., and Schuler, O.: Berechnungsmodul für Erdwärmesonden, *Final report*, Bundesamt für Energie, Switzerland, (1997).

Ingersoll, L., Zobel, O.J., and Ingersoll, A.C.: Heat conduction with engineering, geological and other applications, McGraw-Hill, New York, (1954).

Javed, S., Fahlèn, P., and Claesson, J.: Vertical Ground Heat Exchangers: A Review of Heat Flow Models, Chalmers University of Technology, Goeteborg, Sweden, (2009).

Javed, S., and Claesson, J.: New Analytical and Numerical Solutions for the Short-term Analysis of Vertical Ground Heat Exchanger, *ASHRAE Transactions*, **117**, Part 1, (2011).

Kuebert, M.: Volumen statt Tiefe: Funktion, Anwendungsgebiete und Potenzial von Speichersonden, *Proceedings of 8th Biberacher Geothermietag*, Biberach, Germany, (2011).

Lamarche, L., and Beauchamp, B.: New solutions for the Short-time Analysis of Geothermal Vertical Boreholes, *International Journal of Heat and Mass Transfer*, (2007), 1408-1419.

Lamarche, L.: Short-term Behavior of Classical Solutions for the Design of Ground-source Heat Pumps, *Renewable Energy*, **57**, (2013), 171-180.

Maestre, I.R., Gallero, F.J.G., Gómez, P.Á., and Pérez-Lombard, L.: A new RC and g-function hybrid model to simulate vertical ground Heat Exchangers, *Renewable Energy*, **78**, (2015), 631-642.

Mundry, E.: Über die Lösung der Wärmeleitungsgleichung für den Außenraum eines Zylinders mit kreisförmigen Querschnitt, *International Journal of Heat and Mass Transfer*, **9**, (1966), 189-197.

Paerisch, P., Mercker, O., Oberdorfer, P., Bertram, E., Tepe, R., and Rockendorf, G.: Short-term Experiments with Borehole Heat Exchangers and Model validation in TRNSYS, *Renewable Energy*, **74**, (2015), 471-477.

Steins, C., and Kneer, R.: Vorstellung eines Modellansatzes zum optimierten Betrieb grossvolumiger koaxialer Erdwärmesonden, *Proceeings of German Geothermal Congress*, Essen, German, (2013).

U.S. Energy Information Administration (EIA): Residential Energy Consumption Survey, (2009).

Verein Deutscher Ingenieure (VDI) (Eq.): VDI-Waermeatlas, 11th edition, Springer, (2013).

Yavuzturk, C.: Modeling of Vertical Ground Loop Heat Exchanger for Ground Source Heat Pump Systems, *Doctoral thesis*, Oklahoma State University, USA, (1999).

Yavuzturk, C., and Spitler, J.D.: A Short Time Step Response Factor Model for Vertical Ground Loop Heat Exchangers, *ASHRAE Transactions*, **105** (2), (1999), 475-485.

Young, T.: Development, verification, and Design Analysis of the borehole Fluid Thermal Mass Model for Approximating Short Term Borehole Thermal Response, *Master thesis*, Oklahoma State University, USA, (2001).

Zarrella, A., Scarpa, M., and De Carli, M.: Short time step Analysis of Vertical Ground-coupled Heat exchangers: The approach of CaRM, *Renewable Energy*, **36**, (2011), 2357-2367.